

61

66

68

70

76

78

79

80

81

85

91

93

95

100

102

103

104

106

107

108

110

111

112

RESEARCH ARTICLE

Gearing in a hydrostatic skeleton: the tube feet of juvenile sea stars (*Leptasterias* sp.).

Theodora Po¹, Andres Carrillo¹, Amberle McKee¹, Bruno Pernet², and Matthew J. McHenry¹

ABSTRACT

10

11

12

13

14

15

16

18

20

22

24

25

26

27

28

29

30

31

32

33

34

35

36

37

39

41

42

43

44

45

46

47

48

50

51

52

53

54

55

56

Hydrostatic skeletons, such as an elephant trunk or a squid tentacle, permit the transmission of mechanical work through a soft body. Despite the ubiquity of these structures among animals. we generally do not understand how differences in their morphology affect their ability to transmit muscular work. Therefore, the present study used mathematical modeling, morphometrics, and kinematics to understand the transmission of force and displacement in the tube feet of the juvenile six-rayed star (Leptasterias sp.). An inverse-dynamic analysis revealed that the forces generated by the feet during crawling primarily serve to overcome the submerged weight of the body. These forces were disproportionately generated by the feet at more proximal positions along each ray, which were used more frequently for crawling. Due to a combination of mechanical advantage and muscle mass, these proximal feet exhibited a greater capacity for force generation than the distal feet. However, the higher displacement advantage of the more elongated distal feet offer a superior ability to extend the feet into the environment. Therefore, the morphology of tube feet demonstrates a gradient in gearing along each ray that compliments their role in behavior.

KEYWORDS: Hydrostats, Locomotion, Biomechanics

Introduction

A broad diversity of animals transmit the mechanical work generated by muscles through a soft body. The hydrostatic skeletons that perform this transmission include the tongue of many vertebrates (McClung and Goldberg, 2000; de Groot and van Leeuwen, 2004; Nishikawa et al., 1999), an elephant's trunk (Dagenais et al., 2021; Wilson et al., 1991), a squid's tentacles (Kier, 1982), and the body of an earthworm (Kurth and Kier, 2014; Quillin, 2000). Models of the geometry of these skeletons have provided a basis for inferring their capacity to transmit force and displacement (Clark and Cowey, 1958; Kier, 2012; Ellers et al., 2024). The aim of the present study was to apply this modeling approach to understand the functional implications of variation in morphology within a species. In particular, we used morphometric and kinematic measurements to parameterize a model of the mechanics of the tube feet of the six-rayed star (*Leptasterias* sp.) and to consider the role of the feet in locomotion.

Department of Ecology and Evolutionary Biology, University of California, Irvine, Irvine, CA, 92697, USA

Authors for correspondence: (mmchenry@uci.edu;)

these predictions.

The ability of a structure to transmit force is measured by the

Tube feet are fascinating organs in part due to the broad array of functions that they provide. They serve as soft actuators for locomotion, but they also adhere the body to hard substrates under wave action, facilitate burrowing, transport food to the mouth, and help to pry open hard-shelled prey (Smith, 1947; Paine, 1926). They additionally serve as the primary organ for gas exchange and are capable of multi-model sensing, including mechanoreception and chemoreception (MacGinitie and MacGinitie, 1949; Moore and Thorndyke, 1993; Brewer and Konar, 2005; Shick, 2020; Valentinčič, 1983). Therefore, understanding the mechanics of tube feet informs multiple aspects of the biology of an ecologically important group in marine habitats (Menge and Sanford, 2013).

Tube feet can be highly variable in their anatomy both within and among sea stars and their relatives. The tube foot has a hydraulic skeleton that transmits fluid between two chambers. We will refer to the cylindrical region that protrudes from the body as the stem and the muscular bladder within the foot as the ampulla (Fig. 1). Contraction by the longitudinal muscles within the stem serve to bend and shorten the structure and thereby inflate the ampulla with fluid from its lumen. Shortening by the ampulla muscles reverse this process and thereby extend the stem (Smith, 1947; McCurley and Kier, 1995). The distal end of the stem is shaped like a pointed knob in some species and as a muscular disk in others and the presence of each type correlates with habitat and phylogeny (Blake, 1990; Flammang, 1995; Vickery and McClintock, 2000; Santos et al., 2005). The ampulla also differs among species and may be either elliptical or a shape that approximates a cylinder (Smith, 1946; McCurley and Kier, 1995). Tube foot morphology is highly variable among the echinoderm relatives of sea stars, including the elongated stems that extend beyond the spines of sea urchins, and the stout stems that project from the ray segments of brittle stars (Brusca and Brusca, 2003).

Tube feet vary in their size and shape along each ray. The feet at a proximal position are generally wider and less elongated when extended than those at a distal position. When watching a sea star crawl up the walls of a glass aquarium, the proximal feet exhibit the periodic phases of power and recovery strokes that are characteristic of locomotion, whereas the distal feet move with a gesticulating motion. This motion could aid in sensing the environment and acquiring food particles (Hamilton, 1922; Smith, 1945). The proximal-most feet additionally serve to pass food into the mouth of the sea star. We therefore propose that the ray of a sea star presents a functional gradient along its length, with tube feet serving to generate high force at more proximal positions and greater extension in distal regions. The present study includes tests of these predictions.

mechanical advantage, MA, which is the ratio of output to input

1

² Department of Biological Sciences, California State University Long Beach, Long Beach, CA, 90840, USA

force. In a rigid lever system, MA is equal to the quotient of the in-lever length (distance from the applied force to the fulcrum) to out-lever length (distance from the fulcrum to the point of force application, Alexander, 1983). MA has therefore served as an easily-measured basis for comparing the functional morphology of vertebrate skeletons (Hildebrand et al., 1995; Smith and Savage, 1956). Leverage can be increased either by a greater in-lever or a shorter out-lever length, but a gain in leverage comes at the cost of displacement. The displacement advantage (DA) is defined as the ratio of output to input displacement and it is equal to the inverse of MA in a rigid lever system (Vogel, 1988). It has long been thought that this principle holds true for hydrostatic skeletons (Kier and Smith, 1985), but it was only recently demonstrated mathematically (Ellers et al., 2024). This analysis showed that the inverse relationship between MA and DA requires that the skeleton conserve energy. Therefore, the muscular work applied to the system must be neither stored, nor dissipated, as the structure deforms.

Our experiments focused on the mechanics of crawling in juvenile sea stars in a species of the genus *Leptasterias* (Fig. 2). Juveniles were selected due to their modest number of tube feet (12 per ray), relative to the hundreds present in adult sea stars. This morphological simplicity makes the mechanics of locomotion more experimentally tractable. Our experiments consisted of histological morphometrics of the tube feet and recording the 3D kinematics of the body and tube feet during locomotion to resolve the major forces generated during crawling and the role of individual feet. These measurements served as a basis of a model for the biomechanics of the tube feet.

Materials and methods

Mathematical model of tube-foot mechanics

We used a mathematical model to determine the capacity for the transmission of force and displacement by tube feet, based on morphometric and kinematic measurements. This model is based on a previously-developed theory for hydrostatic skeletons that includes the tube feet of adult sea stars (Ellers et al., 2024). However, the present model differs in a couple of key respects. The ampulla in the animals that we considered are ellipsoidal, which violates the assumed cylindrical shape of some adult tube feet. Also, we accounted for the substantial volumes of the longitudinal muscles and terminal disk at the distal end of the stem, which may be negligible in adult sea stars.

A key factor in tube-foot mechanics is the helical winding of stiff fibers that wrap around the stem. The model assumes that these fibers are effectively inextensible, such that the shape changes of the stem are constrained by the geometry of a helix (Fig. 1C–D). Therefore, the variable length of the stem (l) is proportional to the cosine of the helix angle (θ) :

$$l = n_{\rm h} f \cos \theta, \tag{1}$$

where f is the length of a fiber through a single rotation of the helix, and $n_{\rm h}$ is the number of rotations of the helix along the length (Clark and Cowey, 1958; Chou and Hannaford, 1996) (Fig. 1C). Unlike θ , both f and $n_{\rm h}$ are fixed parameters due to the fibers' high stiffness. It follows that the stem's radius (r) is proportional to the sine of the helix angle:

$$r = \frac{f}{2\pi} \sin \theta. \tag{2}$$

Table 1. Table of symbols.

Symbol	Definition
θ	Helix angle
$\theta_{ m max}$	Helix angle at max. extension
ρ	Density of sea water
σ	Stress in longitudinal muscles
Ω	Stress in ampulla muscles
a	Cross-sectional area of longitudinal muscles
A	Cross-sectional area of ampulla muscles
C	Ampulla circumference
C_{d}	Drag coefficient
D	Body diameter
DA	Displacement advantage
f	Fiber length through one rotation
$F_{ m pull}$	Pulling force
$F_{ m push}$	Pushing force
$F_{ m SW}$	Submerged weight
g	Acceleration of gravity
H	Body height
l	Total stem length
$l_{ m max}$	Total stem length at max. extension
$l_{ m d}$	Length of terminal disk
L	Width of ampulla
m	Body mass
MA	Mechanical advantage
$n_{ m h}$	Number of helix rotations
0	Orientation of substrate
Q	Ray position of a foot
r	Stem radius
R	Ampulla radius
$r_{ m l}$	Stem lumen radius
s	Identity of individual sea star
S	Projected area of the body
t	Thickness of stem muscles
T	Thickness of ampulla muscles
U	Body speed
v	Stem volume
v_{d}	Volume of terminal disk
v_{l}	Volume of stem lumen
$v_{ m m}$	Volume of stem muscles
$v_{ m max}$	Stem volume at max. extension
V	Ampulla volume
w	Total fluid volume
w*	Non-dimensional total fluid volume
$Y_{\rm kine}$	Kinematic variable
Y_{morph}	Morphological variable

The total volume of the stem $(v = \pi l r^2)$ may be rewritten as a function of the helix angle (Eqns. 1 and 2) to yield the following equation (Fig. 1D):

$$v = \frac{n_{\rm h} f^3 \sin^2 \theta \cos \theta}{4\pi}.$$
 (3)

This volume is composed of the sum of volumes of the stem's longitudinal muscles $(v_{\rm m})$, the fluid within the lumen of the stem $(v_{\rm l})$, and the terminal disk $(v_{\rm d})$. As previously observed (Cowey, 1952; Clark and Cowey, 1958), the maximum volume of a fiberwound cylinder is achieved at $\theta_{\rm max} = \arctan\sqrt{2} \approx 54.7$ deg (Fig. 1D).

Determining the gearing of a tube foot requires a model of how changes in the geometry of the ampulla relate to those in the stem. For the stem, it is useful to define the rate of change in length with respect to the change in volume (using Eqns. 1 and 3), as follows

 $2\pi r = f \sin \theta$

Retraction

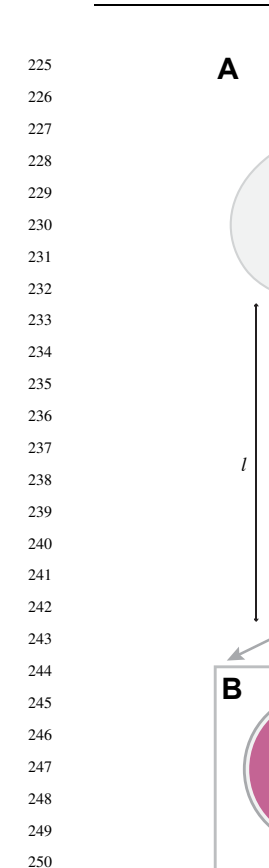
 $\theta_{max} = 54.736^{\circ}$

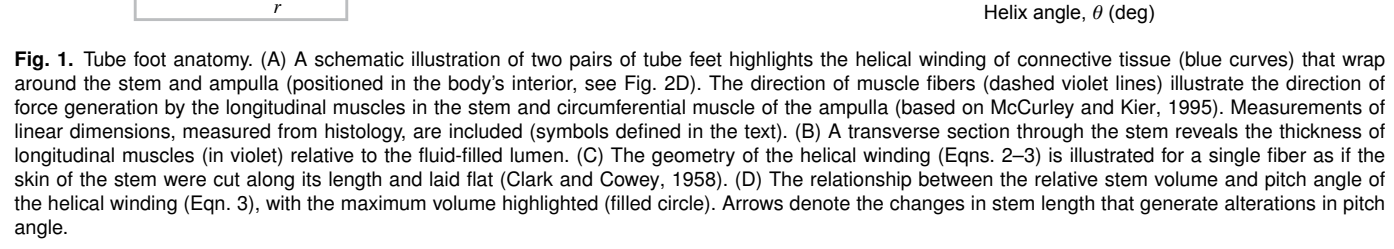
Extension

C

Ampulla

Disk





D

Stem volume, v

0.4

0.3

0.2

2R

Connective

tissue fibers

(Ellers et al., 2024):

$$\frac{dl}{dv_{l}} = \frac{dl/d\theta}{dv_{l}/d\theta} = -\frac{4\pi}{f^{2} \left(3\cos^{2}\theta - 1\right)}.$$
 (4)

Muscles

Note that because of the fixed volumes of the stem muscles and terminal disk, change in the volume of the stem is equivalent to the volume of the lumen (i.e., $dv = dv_l$). We approximate the ampulla with an ellipsoidal shape and hence assume its volume to conform to that geometry (i.e., $V = \pi R L^2/3$, where V, R, and L are respectively the volume, radius and length, Fig. 1A). However, it is necessary to define the ampulla volume with respect to its circumference in one dimension because the circumferential muscles generate the tension by the ampulla. If one assumes that the ampulla's shape is close to that of a sphere, then its circumference may be approximated as circular (i.e., $C = 2\pi R$, where C is the circumference) and the volume may be expressed with respect to the circumference:

$$V = \frac{CL^2}{6}. (5)$$

From the first derivative of this relationship, it is helpful to define how the volume changes with respect to the circumference:

$$\frac{dV}{dC} = \frac{L^2}{6}. (6)$$

 $f\cos\theta$

The DA for a tube foot may be defined as the absolute value of the rate of stem extension with respect to changes in the ampulla's circumference (i.e., DA = |dl/dC|). This relationship may be resolved from the known rate of change in stem length with respect to a change in volume (Eqn. 4), the assumed conservation of mass for an incompressible fluid ($dV = -dv_1$), the derivative of the ampullar volume with respect to circumference (Eqn. 6), and the definition of stem volume enclosed by helical fibers (Eqn. 3):

$$\frac{dl}{dC} = \frac{dl}{dv_1} \frac{dV}{dC} = -\frac{dl}{dV} \frac{dV}{dC}$$

$$\frac{dl}{dC} = \left(-\frac{4\pi}{f^2 (3\cos^2 \theta - 1)} \right) \left(\frac{L^2}{6} \right)$$

$$DA = \left| -\frac{4\pi L^2}{6f^2 (3\cos^2 \theta - 1)} \right|.$$
(7)

Assuming that energy is conserved within the tube foot, the mechanical advantage is equal to the inverse of the displacement

395

396

397

399

401

403

405

406

407

408

409

410

411

412

413

414

415

416

417

418

419

420

421

422

423

424

425

426

427

429

430

431

432

433

434

435

436

437

438

439

440

441

442

443 444

445

446

447

448

337

338

339

340

341

343

344

345

346

347

348

349

350

351

352

353

354

355

356

357

358

359

360

361

362

364

365

366

367

368

369

370

371

372

373

374

375

376

377

378

379

381

382

383

384

385

386

387

388

389

390

391

392

advantage, as previously demonstrated (Ellers et al., 2024):

$$MA = \frac{1}{DA}.$$
 (8)

We accepted this relationship in the present analysis by assuming that the internal viscoelastic resistance to the shape changes of the stem is much smaller than the transmission of work generated by the ampulla.

Animal collection and handling

Adult *Leptasterias* sp. were collected at Baker Beach in Trinidad, CA (41.0488, -124.1236), U.S.A. in May of 2017 and April of 2018. Animals were expressed-shipped to Long Beach, CA, where they were unpacked and held is filtered sea water (Instant OceanTM) with a salinity of 34 ppt, maintained at 16°C. This species was chosen for the present study, in part, because they brood their young until the juvenile stage. Brooding allowed us to collect juveniles without having to culture them through a pelagic larval stage. The juveniles were found on the bodies of adults or within the tanks that held those adults (Fig. 2A).

Morphometrics

Histological sectioning of the bodies of sea stars was performed to collect morphometric measurements of the tube feet. This entailed anesthetizing each animal (10 mmol 1 MgCl₂ for 30 min), transferring them to fixative solution (10% neutral buffered formalin), rinsing in sea water, dehydrating through a series of ethanol solutions (50%, 70%, 90%, and then 100%), embedding in whole body in paraffin, and then sectioning (thickness of 5 μ m). Haemotoxylin and eosin staining was applied to the sections to visualize muscle and connective tissues. Histological sectioning was completed along both the aboral-oral axis, as well as through the body. Our morphometrics consisted of the length (l_{hist}) of the stem lumen, the radius of the stem $(r_{l,hist})$, the length of the terminal disk $(l_{d,hist})$, the thickness of the muscle layer of the stem (t_{hist} , measured at its most thin point), the radius of the ampulla (R_{hist}), and the thickness of the muscular wall of the ampulla (T_{hist}) . We tested the effects of the ray position of the tube feet on the morphometrics. The ray position (Q) was assigned by numbered addresses, starting with the most-proximal tube foot (1) and up to the most-distal position (6, Fig. 2B-C). This test was performed with a generalized linear mix-effects model, assuming a normal distribution, with foot position as a fixed effect and the individual sea star (s) as a random effect. This model is expressed by the following equation, in Wilkinson notation (Wilkinson and Rogers, 1973):

$$Y_{\text{morph}} \sim 1 + Q + (1|s), \tag{9}$$

where $Y_{\rm morph}$ is one of the morphometric measurements. Measurements were performed at 6 positions along the rays, from 3 individuals. Tube-foot pairs were not always both visible and intact. We therefore selected the foot at each position with the most complete view. All statistical analyses were performed in MATLAB.

3D kinematics

We video-recorded the crawling of sea stars to measure the 3D kinematics of the body and tube feet. Crawling was recorded along flat acrylic surfaces with a horizontal, vertical, and inverted (i.e.,

upside-down) orientation to consider the effects of different types of loading upon the feet in a small aquarium (8 cm \times 8 cm wide and 6 cm in height). The cameras (Canon EOS 5D Mark IV with 65mm MP-E macro lens, Canon USA, Huntington, NY and a Sony a7 II with 100mm macro lens, Sony Electronics, San Diego, CA) were oriented at perpendicular perspectives (Fig. 2E) to record locomotion from oral and lateral views. Both cameras recorded a field width of ~ 1 cm at 4K resolution (4096 \times 2160 for the Canon and 3840×2160 for the Sony) at 29.97 fps. The cameras were manually-triggered separately, but we were able to synchronize data extracted from the two perspectives in our post-processing. To facilitate this syncing, we performed a loud clapping of hands at the start of each recording, which was recorded by the microphones of the two cameras. We then analyzed the two audio recordings to determine the latency in timing of the sound between the two cameras. After determining the latency, we interpolated the coordinates extracted from one video to match the frame exposures of the other camera.

We manually-tracked landmarks to measure the kinematics of crawling. Using custom software developed in MATLAB (Mathworks, Natick, MA), we recorded the power strokes of all tube feet from a recording of the oral perspective of the animal. The software prompted the user to select the coordinate for a foot in the frame at which it first contacted the surface, and to input the frame number at which the terminal disk released from the surface. A coordinate was additionally selected for the position of the proximal end of the tube foot upon the body of the sea star. These coordinates, combined with the body kinematics, allowed for calculations of the length and angular position of each tube foot over the duration of a power stroke. This software additionally prompted the user to select coordinates for the red eye spots for each frame of a sequence from the oral and lateral perspectives, as well as the coordinates for the distal positions of the feet from the lateral perspective. Assuming a rigid body, we transformed all coordinates into a body frame-of-reference with its origin positioned at the mouth opening, an x-axis direction in the direction of crawling, a z-axis set perpendicular to the substrate, and the yaxis found by the cross-product of the x- and z-axes, assuming a right-handed coordinate system.

We tested the effects of the substrate orientation, ray position, and individual on kinematic parameters. Our test was performed with a generalized linear mixed-effects model, with ray position and orientation (*O*) as fixed effects and the individual sea star as a random effect. This model is expressed by the following equation:

$$Y_{\text{kine}} \sim 1 + Q + O + (1|s),$$
 (10)

where $Y_{\rm kine}$ is one of the kinematic variables. We performed this test for the duration of the power stroke, assuming a normal distribution. We defined the usage rate as the mean duration of power-strokes by tube feet at a position, divided by the product of the duration of a recording and the total number of feet (12) at that position. Therefore, the usage rate indicates the proportion of time that particular feet are used for locomotion. We tested the effect of ray position on the usage rate using the generalized linear model (Eqn. 10), but assumed a binomial distribution.

Inverse dynamics

We modeled the forces on the body and feet of the sea stars to determine the loads that the feet must overcome to move forward. These calculations were intended as a first-order approximation to

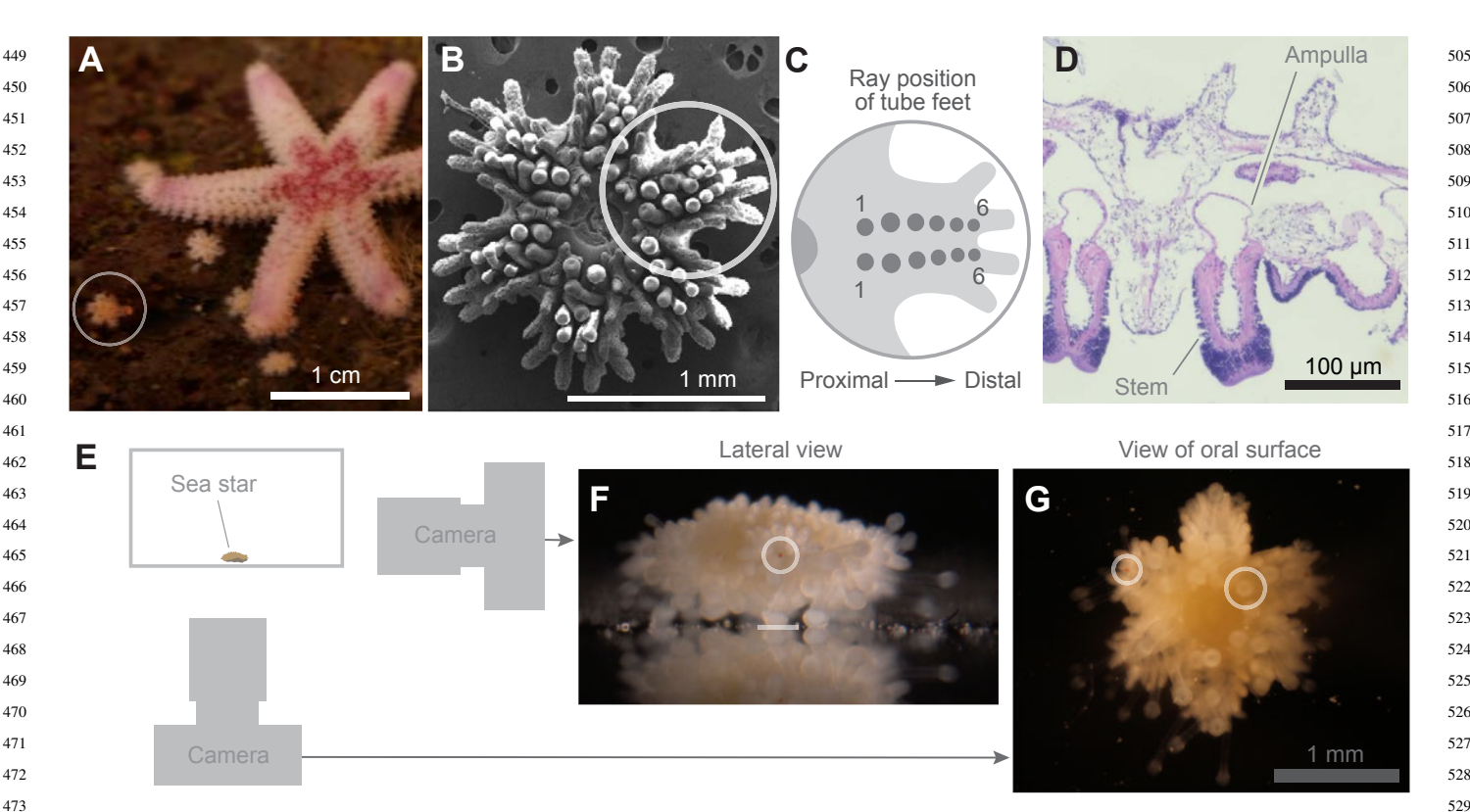


Fig. 2. Morphometric and kinematic measurements the six-rayed star (*Leptasterias* sp.). (A) A single adult and multiple juveniles (one circled). (B) SEM of the oral surface of a juvenile with 6 pairs of tube feet (circled). (C) Schematic of single ray with the position numbers (ordered from proximal to distal) for each pair of feet. (D) A histological section through a pair of rays shows longitudinal sections of two tube feet, each with the ampulla and stem visible (see Fig. 1A). Staining highlights muscle (violet) and nuclei (dark purple). (E) Experimental setup (not drawn to scale) includes a water-filled observation chamber with a single sea star. The locomotion was recorded by cameras that viewed the sea star from lateral and oral perspectives. (F–G) Video stills from a recording are cropped to zoom on the body of a sea star, with features highlighted for clarity. (F) From a lateral view, we measured the position of contact between individual tube feet and the chamber surface (e.g. white line) and the red eye spots (e.g. white circle). (G) The view of the oral surface was used to measure the coordinates of tube feet in contact with the surface (e.g. large circle) and the eye spots (e.g. small circle).

assess the order-of-magnitude of the submerged weight, inertial force, and drag generated by the body motion through still water. We approximated the body as ellipsoidal in shape and found the submerged weight $(F_{\rm SW})$ as the difference between measured wet mass and the buoyancy force on the body. The submerged weight was therefore estimated as follows:

$$F_{\rm SW} = g \left(m - \frac{\pi \rho H D^2}{4} \right),\tag{11}$$

where g is acceleration of gravity, m is body mass, ρ is the density of sea water, H is body height, and D is body diameter (measured from kinematics). The inertial force was calculated for each instant of a kinematic sequence as the product of the mass and body acceleration. Body acceleration and velocity were respectively found as the second and first derivative of a smoothing spline (the 'spaps' function in MATLAB) of position measurements. Body velocity factored into our calculation of drag, which we modeled with the following equation (Batchelor, 1994):

$$F_{\rm d} = \frac{1}{2} C_{\rm d} \rho S U^2, \tag{12}$$

where S is the projected area of the body, assuming an elliptical shape, C_d is the drag coefficient, and U is the forward speed of the

body. We used an empirical measure of the drag coefficient for an ellipsoidal body, given as follows (Hoerner, 1965):

$$C_{\rm d} = \frac{0.014 \left(1 + D\right)}{H} + \frac{1.1H}{D}.\tag{13}$$

As reported in Results, we found the submerged weight to be at least 3 orders-of-magnitude more than the inertial and drag forces. We therefore performed a set of calculations to approximate the forces imposed by the submerged weight on individual feet in horizontal and inverted crawling. We additionally found that the feet most frequently used for crawling are clustered close to the center of the body. We therefore assumed that the weight was evenly distributed among the feet and we hence calculated the vertical component of force generated by each foot to generate this force, given the foot's measured orientation.

Functional analysis of tube foot morphology

We performed a series of calculations on the biomechanical properties of the tube feet that were based on our experimental measurements and mathematical model. These calculations assume that the maximum length $(l_{\rm max})$ that we observed for each stem (achieved during inverted crawling) is equivalent to the theoretical maximum permitted by the helical winding around the stem.

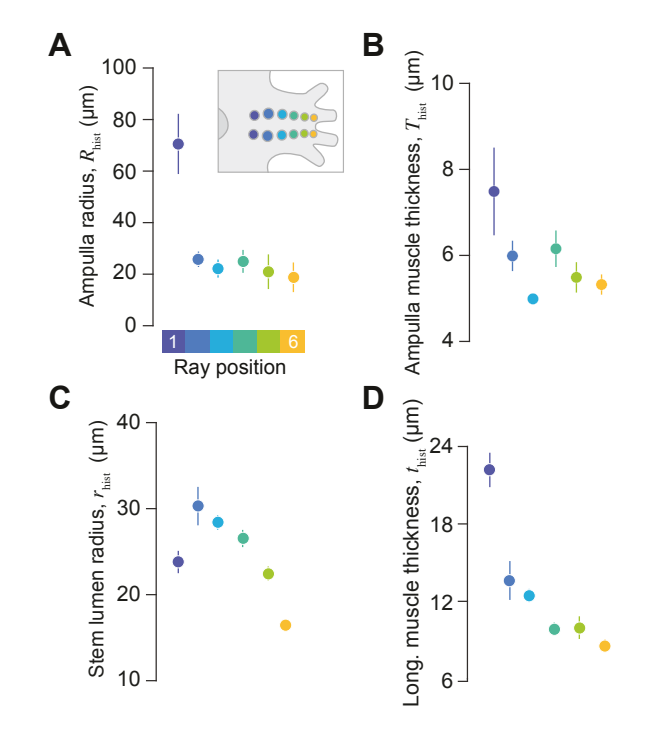


Fig. 3. Morphometrics from histological sections, as a function of position along rays. Ray position is color-coded, with cooler colors for more proximal positions (see inset and horizontal axis in panel A). Mean (\pm 1 SD, N=3 at each position) values of measurements are shown for the (A) ampulla radius, (B) ampulla muscle thickness, (C) stem lumen radius, and (D) longitudinal muscle thickness along the stem. Error bars are smaller than the symbol radius of some points.

In other words, the inverted locomotion was assumed to place the helical fibers in tension to the extent that the stem reached its maximum possible volume (v_{max}) and its corresponding pitch angle $(\theta_{\text{max}} = 54.7 \text{ deg})$. For the purpose of estimating the fiber length, it should not matter whether the podium length in inverted crawling exceeds what is possible from ampulla inflation. Nonetheless, assuming maximum extension permitted a calculation for the length of the average fiber in the stem's helical winding. This fiber length is a key parameter for how the winding changes shape over stem extension. As described above, the fiber length is conventionally parameterized as the product of the length a fiber through a single rotation of the helix and the number of rotations (fn_h , Fig. 1C). We solved for this product using the relationship for the length of a helical volume (Eqn. 1) for θ_{max} and our kinematic measurements of l_{max} . We assumed that each of the tube feet retained the same fiber length between kinematic and histological measurements. This permitted a calculation of the pitch angle (θ_{hist}) from its length (l_{hist}) from histology (using Eqn. 1) as follows:

$$\theta_{\text{hist}} = \text{acos}\left(\frac{l_{\text{hist}}}{f n_{\text{h}}}\right).$$
 (14)

This value for the pitch angle then allowed a calculation of f from histological measurements of the stem radius (r_{hist} , based on Eqn. 2):

$$f_{\text{hist}} = \frac{2\pi r_{\text{hist}}}{\sin \theta_{\text{hist}}}.$$
 (15)

We thereby arrived at values for n_h and f for feet at each ray position.

The histological measurements also provided a basis for approximating the volume of muscles in the ampulla and stem. For the ampulla, the muscle volume was approximated as the product of the surface area of a sphere and the muscle thickness ($V_{\rm m,hist} = 4\pi R_{\rm hist}^2 T_{\rm hist}$). The longitudinal muscle volume was found as the difference between total volume of the stem and the volume of the lumen ($v_{\rm m,hist} = \pi l [r_{\rm hist}^2 - r_{\rm l,hist}^2]$). Our subsequent calculations assumed that the histological volumes approximate the values in vivo and that they remain fixed across tube foot deformations. We thereby calculated the cross-sectional area of muscles to find the stress generated by muscles for a particular load (described below) for the ampulla muscles ($A = V_{\rm m,hist}/[2\pi R]$) and the longitudinal muscles ($a = v_{\rm m,hist}/l$).

We calculated changes in stem geometry across differences in stem length. A critical unknown parameter in these calculations was the volume of fluid within the entire tube foot (w). Presumably due to desiccation, our histological measurements of the lumen volume were found to be less than what was required to maximally extend the stem, as found by kinematics. We therefore performed our calculations at different values for the water volume, calculated as multiples of the stem lumen volume at maximum extension to control for differences in size. The particular water volumes tested were $w = w^*(v_{\text{max}} - v_{\text{m,hist}})$ with the relative volume of $w^* = 1.5$, 2.0, 2.5, or 3.0. For the range of measured stem length values (from kinematics), we found the pitch angle (Eqn. 1), radius (Eqn. 2), total stem volume (Eqn. 3), and lumen volume ($v_1 = v - v_m$). The ampulla volume was found as the difference between the water volume and the stem lumen volume, which permitted a calculation of ampulla radius, assuming an ellipsoidal shape that is spherical at rest (i.e., L=2R). Based on these calculations, the MA (Eqn. 8) and DA (Eqn. 7) were evaluated numerically for variable stem length.

We examined how the tube feet at different positions varied in their capacity to change length. We first evaluated the minimum value for DA (Eqn. 7) with respect to changes in stem length for the feet at each position. We next considered the change in stem length predicted for contraction of the ampulla and longitudinal muscles. For each ray position, we found the distance of this contraction as a 10% strain of the maximum lengths of the ampulla and longitudinal muscles. Due to the variation in DA with the shape of the tube foot, we calculated the effects of that shortening on the range of stem extension at both the maximum and minimum of measured stem lengths for that ray position. These calculations were performed by interpolating numerical values for the relationship between the ampulla circumference and podium length. More simply, the shortening generated by a 10% strain of the longitudinal muscles was taken as 90% of the maximum length of the stem.

We calculated the capacity of feet at each position to generate force. The maximum value for MA (Eqn. 8) within the range of measured stem lengths was evaluated numerically. For both longitudinal and ampulla muscles, we found the stress across the mean cross-sectional area of the muscle generated by the stem to balance the average ground-reaction force generated by tube feet during crawling (0.45 μ N), as determined by our inverse-dynamic analysis (Fig. 5D). The stress by longitudinal muscles ($\sigma = F_{\text{pull}}/a$) is relevant to the pulling forces generated during inverted crawling, where the longitudinal muscles presumably bear most of the body

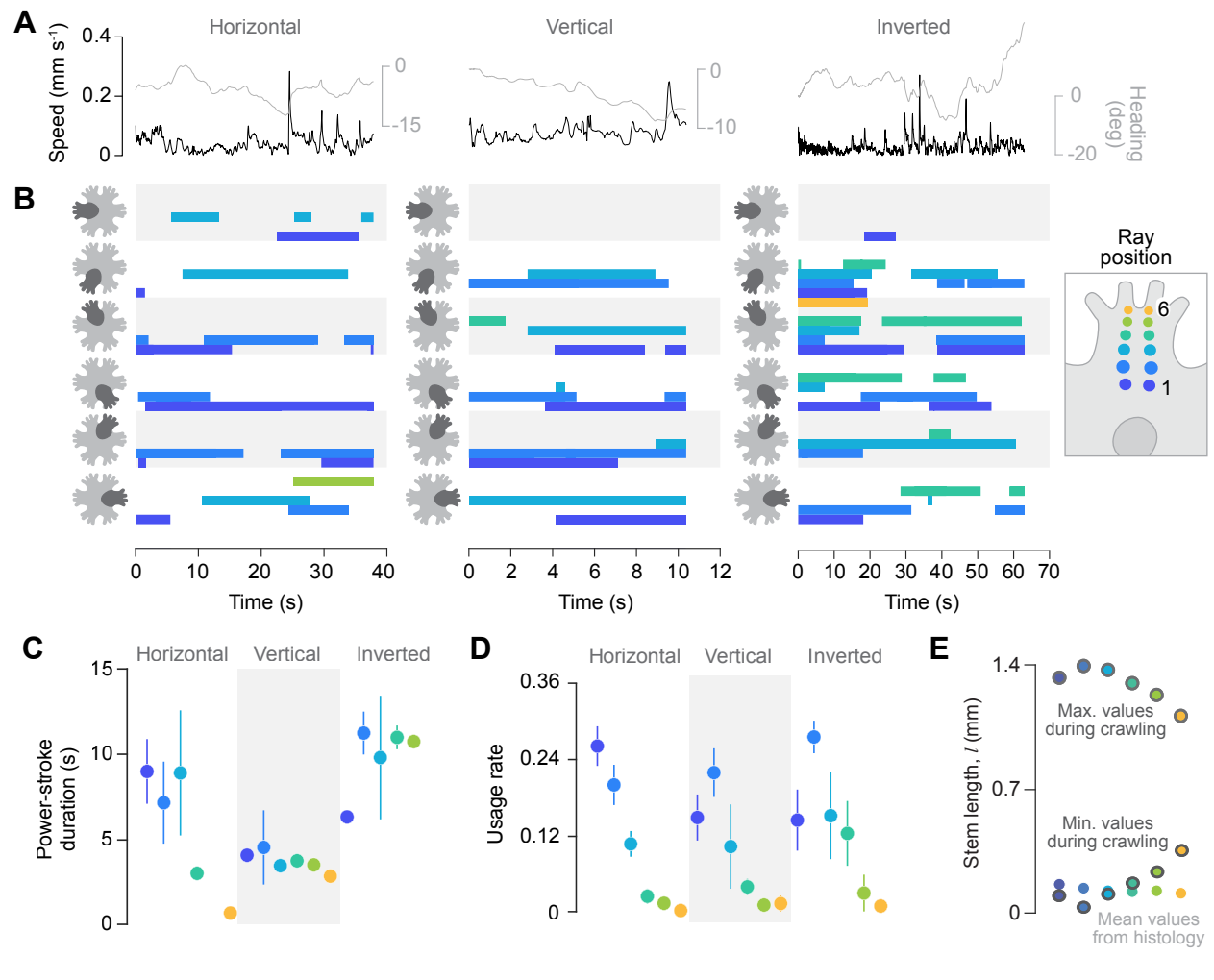


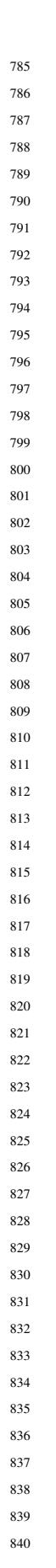
Fig. 4. Kinematics of crawling along surfaces of different orientation. (A–B) Representative kinematic measurements are shown for horizontal (left column), vertical (center column), and inverted (right column) crawling. (A) The speed (in black) and heading (in gray) shown for each experiment. (B) Gait diagrams for the same experiments, with the colored bars indicating the duration that a foot was in contact with the substrate (foot number coded in color, as indicated by legend on the right). The alternating rows (in gray and white) indicate each of the six rays upon which the feet reside, with the particular ray for each row highlighted (dark gray) upon the body (light gray). (C–D) Summary kinematic measurements sea stars (N = 3) crawling along surfaces in the three orientations, with feet color-coded as in the gait diagrams. We found the mean value for each individual and then found the mean (circles) and SEM (error flags) among individuals. (C) The power-stroke duration is the period that a tube foot was in contact with the substrate. (D) The usage rate shows the proportion of time used by tube foot at each position. (E) Maximum and minimum values from measurements of the length of the stem from kinematics (black-lined circles) and from histology (unlined circles).

weight. We calculated the stress generated by the ampulla muscles (Ω) to generate pushing forces that balance the submerged weight, taking MA into account $(\Omega = F_{\text{push}}/[A\text{MA}])$. Conversely, we calculated the forces generated by the tube feet for a maximum stress of 50 kPa, as measured for the longitudinal muscles of *Asterias rubens* previously (Hennebert et al., 2010). The pulling force was determined by the product of this stress and the mean cross-sectional area of the longitudinal muscles. The pushing force was found as the product of the mean cross-sectional area of the ampulla muscles, the muscle stress, and the maximum MA for the foot.

Results

Morphometrics and kinematics

Measurements of the dimensions of the tube feet provided the basis for our analysis of their functional properties. Based on a generalized linear model, we tested whether the position of the tube foot showed significant effects on a number of morphometrics from histological sections (Table S1). The parameters that did not vary significantly among the feet included the foot length and thickness of the ampulla muscle. Significant effects included the radius of the ampulla, and the thickness of longitudinal muscles, which both declined with ray position. The tube feet at Position 1 showed exceptionally large values in these respects. In particular, the mean ampulla radius was 2.73 times greater at Position 1 than Position 2 (Fig. 3A) and longitudinal muscles were larger by 25% (Fig. 3D).



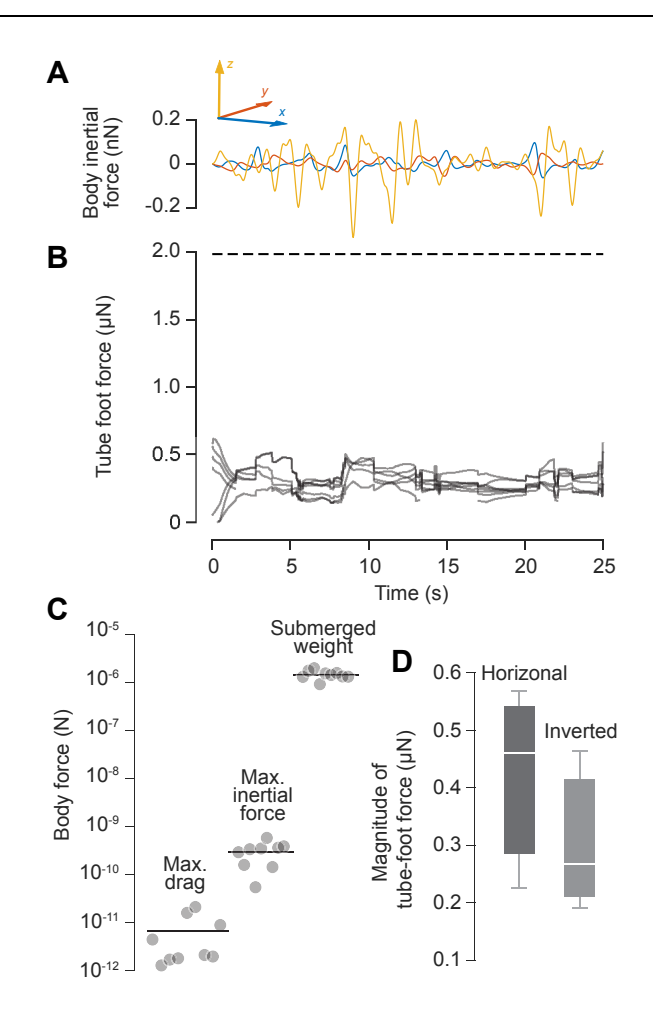


Fig. 5. Force generation by the tube feet during locomotion. (A) Representative recording of the inertial force on the body of a sea star, based on inverse dynamics from kinematic measurements in three translations degrees of freedom. The forward motion is defined along the x-axis (in blue), the y-axis is defined along a lateral dimension (in red), and the z-axis is vertical (in yellow). (B) The force generated by individual tube feet is shown by inverse dynamics, with individual traces for each foot (in gray), with the sum of all feet assumed equal to the submerged weight of the body (horizontal dashed line). These calculations take into account the number of feet in contact with the substrate and their angle with respect to that surface. (C) Estimates for the maximum drag and inertial forces, and submerged weight of the body. (D) The average magnitude of force generated by individual tube feet in horizontal (pushing forces) and inverted locomotion (pulling forces, N=3 for each direction), as determined by inverse dynamics calculations, such as shown in panel B.

In contrast, lumen radius of the feet at Position 1 was smaller than Position 2 by 27% (Fig. 3C), whereas the radius otherwise declined significantly with tube-foot position (Table S1).

We measured the kinematics of crawling over substrates of different orientations to assess potential differences in the behavioral role between feet at different positions. Sea stars moved in a generally linear path, with oscillations in speed and heading that roughly corresponded to the attachment and detachment events of the tube feet (Fig. 4A–B). According to a generalized mixed-effects model, the duration of the power stroke did not vary significantly with the ray position (P=0.47), or substrate orientation (P=0.12,

N=3, Fig. 4C). However, the tube feet did vary significantly (P<0.001,N=3) in their usage among the different positions (Fig. 4D). The usage rate was calculated as the total duration of all power strokes for feet at a particular position, divided by the product of the total number of feet along the ray and duration of a recording. We found that the usage rate was substantially higher in the three most-proximal feet than in the more distal feet. For example, the feet at Position 2 were used 8.3 times more frequently than the feet at Position 4 in horizontal crawling. The substrate orientation showed no significant (P=0.37,N=3) effect on the usage rate, though the feet at Position 2 were used more frequently than Position 1 in vertical and inverted crawling (Fig. 4D). As explained below, these prevailing morphological trends have functional implications.

Inverse dynamics

We performed an inverse dynamic analysis to resolve the major loads on the tube feet during crawling. From measurements of the 3D kinematics of the body, we calculated the torques and forces collectively generated by the feet to respectively rotate and translate the body mass (Fig. 5A–C). Upon performing these calculations for all experiments, we found that the inertial forces were effectively negligible compared to the submerged weight of the body (Fig. 5C). In particular, the mean submerged weight $(1.5\mu\mathrm{N}, N=3)$ was 5000-times greater than the maximum inertial force $(0.3~\mathrm{nN}, N=3)$. In addition, the inertial force was 43-times greater than the maximum drag on the body $(6.8~\mathrm{pN}, N=3)$. Therefore, the forces generated by the tube feet are overwhelmingly applied towards supporting the submerged weight of the body.

We used our measurements of the 3D kinematics of individual tube feet to estimate the forces generated to balance the body's submerged weight. This consists of pushing forces for horizontal crawling and pulling forces against the substrate for inverted crawling. We found that these two orientations yielded similar values (P=0.44, Students two-tailed t-test, N=3) for tube-foot force (Fig. 5D), suggesting that differences in the numbers of tube feet and orientation did not yield a substantially different magnitude in force.

Mathematical modeling

The functional morphology of tube feet at different positions was ultimately resolved through an application of our mathematical model with parameter values provided by our morphological and kinematic measurements. These calculations incorporated morphometrics from histology to resolve the fiber length of the podium's helical winding (Eqn. 15) and the volume's of the muscle and lumen (described above). However, we varied the fluid volume within the tube foot in our calculations to compensate for the artifacts due to desiccation from our histological measurements. These volumetric differences affected only the ampulla due to the helical winding that constrains the dimensions of the stem. The feet were smaller in volume and had a more elongated stem at the distal positions (Fig. 6A-B). Nonetheless, all feet exhibited a similar maximum length (Fig. 3D), which yielded similar predictions in helix angle, despite the differences in stem radius among the positions (Fig. 6C–D).

The tube feet were found to exhibit variable gearing over the extension of the stem. As the stem approached its maximum extension, the DA increased exponentially and MA declined to zero

Fig. 6. Simulated changes in the geometry of tube feet, based on morphometrics and kinematics, organized in columns for each tube foot. (A) Schematic illustrations show the predicted changes in the tube foot dimensions at the minimum and maximum stem lengths, measured from kinematics (Fig. 3D). (B–F) Calculations of the shape changes and mechanical properties that vary with stem length, according to our measurements and mathematical model for the stem (gray curves) and ampulla (colored curves) for a range of relative fluid volumes (legend in upper left). Changes in tube foot geometry, such as (B) the fluid volume and (C) helix angle, and (D) radius of both chambers, which determine the (E) DA (Eqn. 7) and (F) MA (Eqn. 8) of each tube foot.

(Fig. 6E–F). Therefore, all of the feet were best at generating force at short stem length and offered the greatest rate of extension at greater lengths. The feet at different positions did present variations on this theme. The feet increased in their minimum DA (Fig. 7A) and decreased in maximum MA (Fig. 8A) at more distal positions. These trends in the transmission of mechanical work favored force generation in proximal feet and stem displacement at distal positions along the ray.

The forces generated by tube-foot muscles depends on their cross-sectional area. Our analysis of muscle stress focused on a single load $(0.45\,\mu\mathrm{N})$ that approximates the average force generated by tube feet during crawling (Fig. 5D). The stress upon the longitudinal muscles (e.g., used during inverted crawling) is inversely proportional to their cross-sectional area and hence increased with ray position (Fig. 8E). This trend favored the more

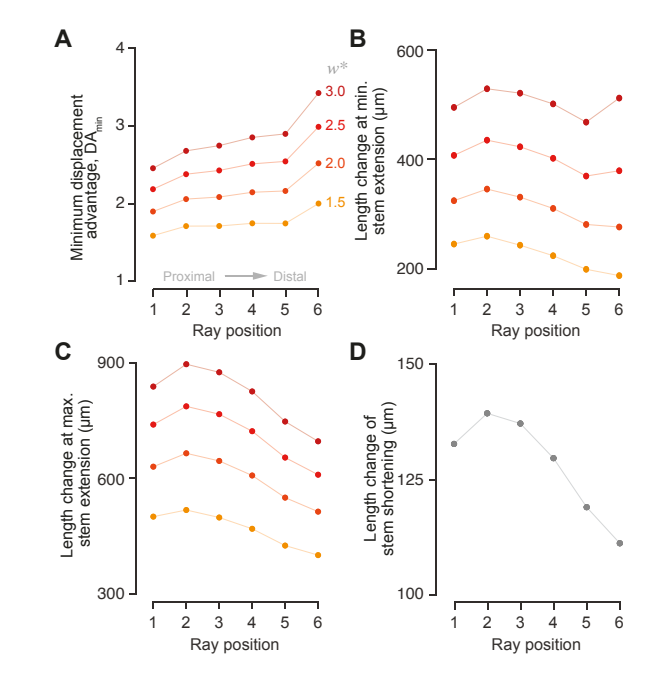


Fig. 7. Predictions of the mechanical properties related to the displacement of tube feet at different positions. Values for the (A) minimum DA across changes in stem extension (Fig. 6E). (B–D) Changes in stem length generated by 10% strain in the (B–C) ampulla muscles and (D) longitudinal muscles. The range of stem length changes were calculated around the (B) minimum length of the stem and (C) and the maximum length of the stem. (B–C) The length changes in the stem generated over extension, generated by contraction of the ampulla muscles. (D) The range of shortening calculated for the stem due to contraction of the longitudinal muscles.

proximal feet generating higher forces than the distal feet. A similar trend is apparent for the ampulla muscles, but those stresses are inversely proportional to both cross-sectional area and MA (Fig. 7B, D, F). The stress upon ampulla muscles was about 3 orders-of-magnitude greater than those predicted for the longitudinal muscles due both to MA and their smaller cross-sectional area.

Discussion

We used mathematical modeling, morphometrics, and kinematics to explore the mechanical properties of tube feet in a juvenile sea star (*Leptasterias* sp.). This investigation revealed that the morphology of the feet vary with their position along the length of each ray, with the proximal feet being larger (Fig. 3) and morefrequently used in locomotion (Fig. 4). Through the combined effects of MA, DA, size, and muscle mass, the tube feet exhibit a greater capacity for force generation at proximal positions. The smaller distal feet exhibit a relatively high DA and therefore are geared for extending into the environment. These results demonstrate how variation in the morphology of hydrostatic skeleton can affect the generation and transmission of mechanical work.

The mechanics of tube feet are relatively simple during inverted crawling. The longitudinal muscles in the stem likely generate the tensile forces that directly support the body's submerged weight (Figs. 5D, 9C–D). Because no force transmission is required for this task, the stress encountered by the muscles is simply the ratio of the load and the cross-sectional area of the muscle. That area

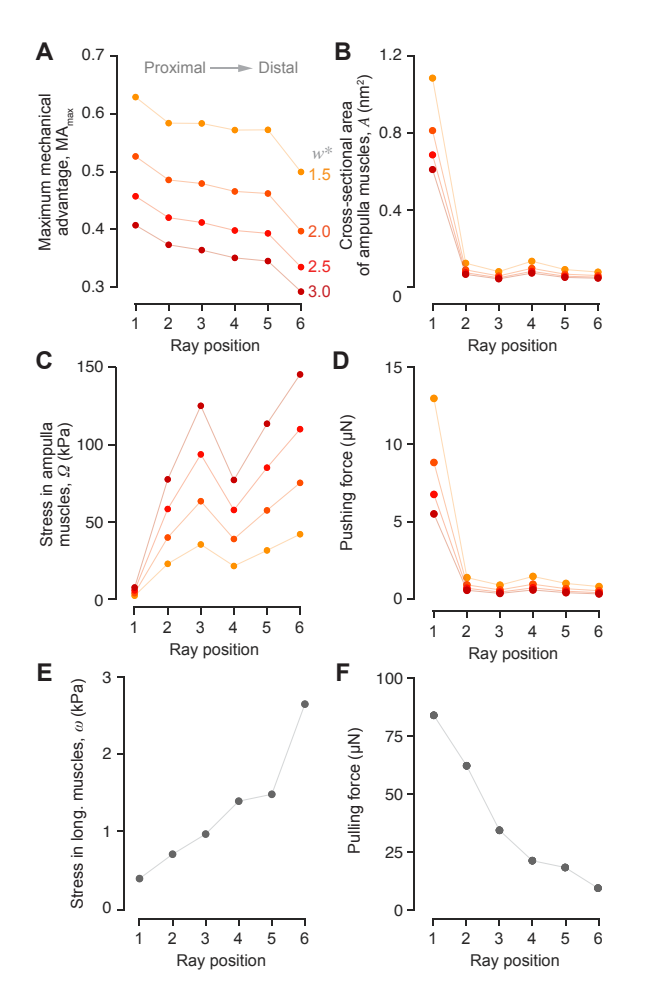


Fig. 8. Summary predictions of forces generation by tube feet at different positions. (A) The maximum MA was calculated with respect to differences in shape (Fig. 6) for different values of the relative fluid volume (w^* , color coding). (B) Differences in the cross-sectional area of ampulla muscles depends on their thickness and the ampulla radius (Fig. 3A–B). (C) Muscle stress generated for the average load to support the submerged weight of the body $(0.45\,\mu\text{N})$, found by dividing that force by the cross-sectional area of that muscle (shown in C). (D) The pushing force generated by the ampulla muscles for a stress of 50 kPa, which depends on both the cross-sectional area of the muscle and MA. (E) The stress in longitudinal muscles to support the submerged weight in inverted crawling and (F) the pulling force generated by those muscles at a stress of 50 kPa.

decreases monotonically with ray position, it follows that the stress to support the submerged weight to increase in the opposite direction (Fig. 7E). It bears mentioning that these stresses are rather small. The isometric stress of longitudinal muscles has been measured in sea star tube feet as been measured at more than an order-of-magnitude greater (48–62 kPa, Hennebert et al., 2010), which is higher than what was previously found in sea cucumber longitudinal body wall muscles (20 kPa, Takemae et al., 2009). The pulling forces predicted for these muscles greatly exceeds the submerged weight of the body (Fig. 8F). Therefore, the longitudinal muscles appear to be overbuilt for inverted crawling, but instead may be better matched to other mechanical tasks. For example, they aid in adhering to hard surfaces under wave action and serve to pry open hard-shelled prey in adults (Paine, 1926; Smith, 1947).

Fig. 9. Schematic illustration of action by tube feet during crawling favored by the present results. (A–D) The submerged weight (red arrow) is the dominant load (Fig. 5C) that is balanced by the ground-reaction forces (orange arrows) generated in response to action by the tube feet. (A–B) For horizontal crawling, the reaction forces are generated primarily by pushing forces that are powered by (B) the ampulla muscles. In contrast, (C–D) the pulling reactive forces for inverted crawling are generated by the longitudinal muscles along the stem. (E) A schematic illustration of the tube feet from an oral view, with (F) a detail of a single ray with the feet color-coded based on their geometry favoring high MA (in green) or high DA (in purple, Figs. 7A, 8A). Despite the spatial pattern in MA, (G) the maximum pushing force is predicted to decrease monotonically along the length of the ray (Fig. 8D), with the most-proximal force generating the highest force, due to the muscle mass of the ampulla (Fig. 3A–B).

Crawling along a horizontal surface requires that each tube foot transmit the contractions generated by ampulla muscles to extend its stem. Shortening by these muscles transfers fluid into the stem, where it acts to expand its volume and transmit pushing forces to the substrate (Fig. 9A–B). The helical winding around the stem constrains how a volume expansion changes its radius (Eqn. 2) and length (Eqn. 1, McCurley and Kier, 1995) and these factors are encapsulated in the equation for DA (Eqn. 7). For ray positions 2 through 6, the radius and muscle thickness of both the ampulla and stem decrease at more distal positions along the ray (Fig. 3, Tables S1, S2). The trend in dimensions along the ray generate an increase

in the minimum DA with position (Fig. 7A), which helps provide more amplification of ampulla muscle shortening in the length changes of the stem. However, the extension of the stem additionally depends on the size of the tube foot and ampulla muscles. Due to these factors, the extension of the feet is actually greater at more proximal positions along the ray (Fig. 7B–C). Nonetheless, DA does enhance the ability of the small distal tube feet to extend and thereby enhance the ability to grasp food particles and to sense the environment with contact for tactile and chemical cues. Consistent with this idea, we found that the feet at positions 5 and 6 rarely contributed to locomotion (Fig. 4), but were instead splayed outward. This behavior may be readily observed in adults of different species and is among the classic observations of tube feet (Hamilton, 1922; Smith, 1945).

The tube feet additionally serve to transmit pushing forces. Force generated by the ampulla muscles pressurize the fluid, and that pressure is transmitted to the lumen of the stem. In addition to constraining the dimension of the stem, tension in the helical fibers provides a source of internal resistance to the pushing force (Ellers et al., 2024) that supports the submerged weight during horizontal crawling (Fig. 9A-B). As with rigid lever systems, the MA of a hydrostatic skeleton is inversely related to DA (Eqn. 8), if the system conserves energy. As a consequence, the trend in DA from Positions 1 to 6 is mirrored by an inverse pattern in MA (Figs. 7B, 9F). This is beneficial for locomotion, given the high usage of the proximal feet during crawling (Eqn. 4, Ellers et al., 2021). However, even the highest values for MA among the feet are less than unity, which means that the ampulla muscles generate more force than the pushing force generated by the stem. The combined factors of MA and the cross-sectional area of the thin ampulla muscles (Fig. 3B) predict stresses (Fig. 8C) that meet or exceed the isometric stress previously reported (48–62 kPa, Hennebert et al., 2010). This suggests that the ampulla operates near its maximal capacity and that the fluid volume within the tube feet operates at the lower range of our estimates.

The functional differences among tube feet that we have observed in *Leptasterias* sp. are reminiscent of the tube feet of sea urchins and sand dollars (Class Echinoidea). Sea urchins possess morphologically-distinct categories of tube feet that are associated with different functions (Nichols, 1959; Telford et al., 1985; Santos et al., 2005). The aboral surface of a sea urchin's body generally features respiratory tube feet that specialize in gas exchange, with a ciliated lumen that is continuous with the water vascular system. 'Suckered' (i.e., secondary or accessory) tube feet are distributed in large regions of the body, where they may extend beyond the spines to grasp food particles and contribute to locomotion. These feet are capable of passing food between neighboring feet to transport it to the mouth (Telford et al., 1985) and can be further categorized by their length, ultrastructural trait features of their distal tip, and role played in food transport (Telford et al., 1983). Buccal tube feet are positioned around the mouth, where they complete the transport of food particles. These feet are stronger and stiffer than the others and additionally perform locomotion and are critical for adhesion to hard substrates (Leddy and Johnson, 2000). The present results indicate functional variations of a more subtle variety among sea stars than found in urchins, but our measurements also reflect similar mechanical specialization with ray position.

In summary, the tube feet within the body of a juvenile *Leptasterias* sp. are anatomically variable in ways that affect their ability to extend and generate force. In particular, the feet are smaller at

more distal positions (Fig. 1) and differ in shape in a manner that increases DA and decreases MA (Figs. 7A, 8A). The exception to this pattern is the proximal-most feet, which have the highest DA along the ray. In spite of this gearing, the force output is predicted to be greatest by the most-proximal feet due to the muscles in the ampulla (Fig. 8D), and these are are the most-frequently used feet for crawling (Fig. 4D). Therefore, the gearing of the tube feet is a factor in how mechanical work is transmitted by the tube feet, but this aspect of morphology may be altered by the force-generation capacity of muscle.

Competing interests

We declare we have no competing interests.

Author contributions

MJM designed the study. The experiments were performed through a collective effort among all authors, spearheaded by AC. TP and AC collected the kinematic and morphometric data. BP facilitated the experiments and availability of animals. MJM and TP wrote the manuscript, with input from all authors.

Acknowledgements

PE Bourdeau generously collected and shipped us the animals for experimentation. Essential contributions were made by O. Ellers and A. Johnson in the development of mathematical models of tube feet. K. Kanso, S. Heydari, and two anonymous reviewers provided helpful suggestions throughout.

Funding

MJM is supported by grants from NSF (IOS-2034043) and ONR (N00014-19-1-2035, N00014-22-1-2655).

REFERENCES

- Alexander, R. M. (1983). Animal Mechanics. Seattle: Univ. of Washington Press
- **Batchelor, G. K.** (1994). *An Introduction to Fluid Dynamics*. Cambridge: Cambridge Univ. Press, 615 pp.
- **Blake, D. B.** (1990). Adaptive zones of the class asteroidea (echinodermata). *Bull. Mar. Sci.* **46**, 701–718.
- **Brewer, R. and Konar, B.** (2005). Chemosensory responses and foraging behavior of the seastar pycnopodia helianthoides. *Mar. Biol.* **147**, 789–795.
- **Brusca, R. C. and Brusca, G. J.** (2003). *Invertebrates*. Sunderland, MA: Sinauer Assoc. Inc.
- Chou, C.-P. and Hannaford, B. (1996). Measurement and modeling of mckibben pneumatic artificial muscles. *IEEE Transactions on robotics and* automation 12, 90–102.
- Clark, R. B. and Cowey, J. B. (1958). Factors controlling the change of shape of certain nemertean and turbellarian worms. *J. Exp. Biol.* **35**, 731–748.
- **Cowey, J.** (1952). The structure and function of the basement membrane muscle system in amphiporus lactifloreus (nemertea). *J. Cell Sci.* **3**, 1–15.
- Dagenais, P., Hensman, S., Haechler, V. and Milinkovitch, M. C. (2021).
 Elephants evolved strategies reducing the biomechanical complexity of their trunk. *Curr. Biol.* 31, 4727–4737.
- **de Groot, J. H. and van Leeuwen, J. L.** (2004). Evidence for an elastic projection mechanism in the chameleon tongue. *Proc. Roy. Soc. B* **271**, 761–770.

- Ellers, O., Ellers, K.-I., Johnson, A. S., Po, T., Heydari, S., Kanso, E. and McHenry, M. J. (2024). Soft skeletons transmit force with variable gearing. *J. Exp. Biol.* **227**, jeb246901.
- Ellers, O., Khoriaty, M. and Johnson, A. S. (2021). Kinematics of sea star legged locomotion. *J. Exp. Biol.* **224**, jeb242813.
- **Flammang, P.** (1995). Fine structure of the podia in three species of paxillosid asteroids of the genus luidia (echinodermata). *Belgian j. zool.* **125**, 125–125.
- **Hamilton, W. F.** (1922). Coördination in the starfish. ii. locomotion. *J. Comp. Psychol.* pp. 61–75.
- Hennebert, E., Haesaerts, D., Dubois, P. and Flammang, P. (2010). Evaluation of the different forces brought into play during tube foot activities in sea stars. *J. Exp. Biol.* **213**, 1162–1174.
- **Hildebrand, M., Goslow, G. E. and Hildebrand, V.** (1995). Analysis of vertebrate structure .
- **Hoerner, S. F.** (1965). *Fluid-Dynamic Drag*. Brick Town, NJ: Hoerner Fluid Dynamics.
- **Kier, W. M.** (1982). The functional morphology of the musculature of squid (loliginidae) arms and tentacles. *J. Morph.* **172**, 179–192.
- Kier, W. M. (2012). The diversity of hydrostatic skeletons. J. Exp. Biol. 215, 1247–1257.
- Kier, W. M. and Smith, K. K. (1985). Tongues, tentacles and trunks: the biomechanics of movement in muscular-hydrostats. *Zool. J. Linnean Soc.* 83, 307–324.
- **Kurth, J. A. and Kier, W. M.** (2014). Scaling of the hydrostatic skeleton in the earthworm Lumbricus terrestris. *J. Exp. Biol* **217**, 1860–1867.
- Leddy, H. A. and Johnson, A. S. (2000). Walking versus breathing: mechanical differentiation of sea urchin podia corresponds to functional specialization. *Biol. Bull.* 198, 88–93.
- MacGinitie, G. E. and MacGinitie, N. (1949). *Natural history of marine animals*. New York: McGraw-Hill.
- **McClung, J. R. and Goldberg, S. J.** (2000). Functional anatomy of the hypoglossal innervated muscles of the rat tongue: a model for elongation and protrusion of the mammalian tongue. *Anat. Rec.* **260**, 378–386.
- **McCurley, R. S. and Kier, W. M.** (1995). The functional morphology of starfish tube feet: the role of a crossed-fiber helical array in movement. *Biol. Bull* **188**, 197–209.
- Menge, B. A. and Sanford, E. (2013). Ecological role of sea stars from populations. In *Starfish: biology and ecology of the Asteroidea* (ed. J. M. Lawrence). Baltimore, MD: Johns Hopkins Univ. Press.
- Moore, S. J. and Thorndyke, M. C. (1993). Immunocytochemical mapping of the novel echinoderm neuropeptide salmfamide 1 (s1) in the starfish asterias rubens. *Cell Tiss. Res.* **274**, 605–618.
- **Nichols, D.** (1959). The histology and activities of the tube-feet of echinocyamus pusillus. *Quart J Micro Sci* **100**, 539–555.
- **Nishikawa, K. C., Kier, W. M. and Smith, K. K.** (1999). Morphology and mechanics of tongue movement in the african pig-nosed frog hemisus marmoratum: a muscular hydrostatic model. *J. Exp. Biol.* **202**, 771–780.
- **Paine, V. L.** (1926). Adhesion of the tube feet in starfishes. *J. Exp. Zool.* **45**, 361–366.
- **Quillin, K.** (2000). Ontogenetic scaling of burrowing forces in the earthworm Lumbricus terrestris. *J. Exp. Biol.* **203**, 2757–2770.

- Santos, R., Haesaerts, D., Jangoux, M. and Flammang, P. (2005). Comparative histological and immunohistochemical study of sea star tube feet (Echinodermata, Asteroidea). *J. Morph.* **263**, 259–269.
- Shick, J. M. (2020). Respiratory gas exchange in echinoderms. In *Echinoderm*studies, pp. 67–110. CRC Press.
- Smith, J. E. (1945). The role of the nervous system in some activities of starfish. *Biol. Rev.* **20**, 29–43.
- Smith, J. E. (1946). The mechanics and innervation of the starfish tube foot ampulla system. *Phil. Trans. Roy. Soc. B: Biol. Sci.* 232, 279–310.
- Smith, J. E. (1947). The activities of the tube feet of Asterias Rubens L: I.

 The mechanics of movement and of posture. *J. Cell Sci.* s3-88, 1–14.
 - Smith, J. M. and Savage, R. J. (1956). Some locomotory adaptations in mammals. *Zool. J. Linnean Soc.* **42**, 603–622.
 - **Takemae, N., Nakaya, F. and Motokawa, T.** (2009). Low oxygen consumption and high body content of catch connective tissue contribute to low metabolic rate of sea cucumbers. *Biol. Bull.* **216**, 45–54.
 - **Telford, M., Harold, A. S. and Mooi, R.** (1983). Feeding structures, behavior, and microhabitat of echinocyamus pusillus (echinoidea: Clypeasteroida). *Biol. Bull.* **165**, 745–757.

- **Telford, M., Mooi, R. and Ellers, O.** (1985). A new model of podial deposit feeding in the sand dollar, mellita quinquiesperforata (leske): the sieve hypothesis challenged. *Biol. Bull.* **169**, 431–448.
- **ValentinčIč, T.** (1983). Innate and learned responses to external stimuli in asteroids. In *Echinoderm studies 1*, pp. 111–137. CRC Press.
- Vickery, M. S. and McClintock, J. B. (2000). Comparative morphology of tube feet among the asteroidea: phylogenetic implications. *Am. Zool.* 40, 355–364.
- **Vogel, S.** (1988). *Life's Devices: The Physical World of Animals and Plants*. Princeton, NJ: Princeton University Press.
- Wilkinson, G. N. and Rogers, C. E. (1973). Symbolic description of factorial models for analysis of variance. J. Roy. Stat. Soc. 22, 392–399.
- Wilson, J., Mahajan, U., Wainwright, S. and Croner, L. (1991). A continuum model of elephant trunks. *J. Biomech. Engineer.* **113**, 79–84.